Environmental Science & Technology

Article

pubs.acs.org/est

Elucidation of the Molecular Determinants for Optimal Perfluorooctanesulfonate Adsorption Using a Combinatorial Nanoparticle Library Approach

Yin Liu,[†,‡] Gaoxing Su,[†] Fei Wang,[§] Jianbo Jia,[†] Shuhuan Li,[†] Linlin Zhao,[⊥] Yali Shi,[‡] Yaqi Cai,[‡] Hao Zhu,[⊥,#] Bin Zhao,[‡] Guibin Jiang,[‡] Hongyu Zhou,*[,¶] and Bing Yan*[,†]

[†]School of Environmental Science and Engineering, Shandong University, Jinan, Shandong 250100, China

[‡]Research Center for Eco-Environmental Science, Chinese Academy of Sciences, Beijing 100085, China

[§]Jinan Entry-Exit Inspection and Quarantine Bureau, Jinan, Shandong 250014, China

[¶]School of Environment, Jinan University, Guangzhou, Guangdong 510632, China

[⊥]Department of Chemistry, Rutgers University, Camden, New Jersey 08102, United States

[#]The Rutgers Center for Computational and Integrative Biology, Rutgers University, Camden, New Jersey 08102, United States

Supporting Information

ABSTRACT: Perfluorooctanesulfonate (PFOS) persistently accumulates in the environment and in humans, causing various toxicities. To determine the key molecular determinants for optimal PFOS specificity and efficiency, we designed and synthesized a combinatorial gold nanoparticle (GNP) library consisting of 18 members with rationally diversified hydrophobic, electrostatic, and fluorine−fluorine interaction components for PFOS bindings. According to our findings, the electrostatic and F−F interactions between PFOS and nanoparticles are complementary. When F−F attractions are relatively weak, the electrostatic interactions are dominant. As F−F interactions increase, the electrostatic contributions are reduced to as low as 20%, demonstrating that F−F binding may overpower even electrostatic interactions. Furthermore, F−F interactions (28−79% binding efficiency) are 2-fold stronger than regular hydrophobic interactions (15−39% binding efficiency) for PFOS adsorption, explaining why these novel PFOS-binding nanoparticles are superior to other conventional materials based on either hydrophobic or electrostatic binding. The PFOS adsorption by the optimized nanoparticles performs well in the presence of ionic interferences and in environmental wastewater. This library mapping approach can potentially be applied to recognition mechanism investigation of other pollutants and facilitate the discovery of effective monitoring probes and matrices for their removal.

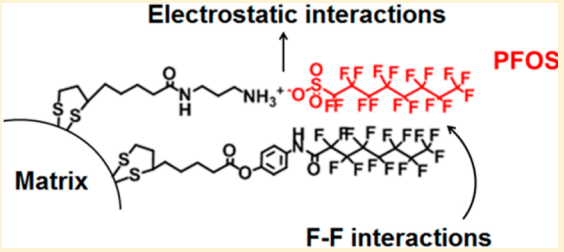

INTRODUCTION

Perfluorooctanesulfonate (PFOS) is one of the persistent organic pollutants (POPs) included in the Stockholm Convention.[1] This pollutant is widely distributed in the environment. It has been found in the Tennessee River,[2] the Baltic Sea,[3] Tokyo Bay,[4] and dolphins from the Brazilian Coast.[5] In addition to its wide distribution and accumulation, it has also been found in humans, such as in cord blood,[6,7] breast milk,[8] and human plasma.[9,10] The accumulation of PFOS in humans may cause significant toxicity. Abnormal sexual development in children has been correlated with their serum concentration of PFOS.[11] The concentration of PFOS in cord serum is also linked to reductions of the birth weight, ponderal index, and head circumference in newborns.[12] Danish children born to mothers with higher plasma PFOS levels are more likely to start sitting without support at a later age than those born to mothers with lower PFOS levels.[13]

Because of its high stability, the degradation of PFOS is difficult to achieve with current pollutant treatment methods.[14,15] The removal of PFOS from an aqueous phase often involves nonspecific adsorptions, such as anion exchange[16,17] and hydrophobic interactions.[18,19] However, adsorbents, such as activated carbon,[20,21] zeolites,[22] and sludge,[23,24] do not show any selectivity for PFOS. Molecularly imprinted polymers (MIPs) offer improved selectivity.[25] However, this method has a relatively long equilibrium time and a lower binding capacity. Using perfluorinated magnetic mesoporous microspheres for extraction of PFOA and PFOS from water and biological samples showed that a short equilibrium time and good selectivity could be achieved.[26−28] Other than mesoporous microspheres, perfluorinated silica gels have also been used as liquid chromatography stationary phases for PFOS adsorption.[29−32] From these studies, F−F interaction is an important

Received: March 30, 2017
Revised: May 18, 2017
Accepted: May 24, 2017
Published: May 24, 2017

DOI: 10.1021/acs.est.7b01635
Environ. Sci. Technol. 2017, 51, 7120−7127

Table 1. Chemical Structure and Numbering of the Combinatorial GNP Library

		R_1		
		SN1	SN2	SN3
R_2	SH1 $-CH_2(CH_2)_2CH_3$	**H1**	**H2**	**H3**
	SH2 $-CH_2(CH_2)_5CH_3$	**H4**	**H5**	**H6**
	SH3 $-CH_2(CH_2)_7CH_3$	**H7**	**H8**	**H9**
	SF1 $-CF_2(CF_2)_2CF_3$	**F1**	**F2**	**F3**
	SF2 $-CF_2(CF_2)_5CF_3$	**F4**	**F5**	**F6**
	SF3 $-CF_2(CF_2)_7CF_3$	**F7**	**F8**	**F9**

attribute to PFOS binding. However, the role of positive charge and the interplay between the charge and F−F interactions also need to be addressed. Because of the eco-environmental and toxicological importance of this issue, the onsite detection and effective removal of PFOS have become imperative tasks, especially in drinking water sources that contain a low concentration of PFOS. To achieve these objectives, a fundamental understanding of the molecular interactions for PFOS adsorption is essential.[33]

Compared to a one-at-a-time trial-and-error approach, the combinatorial nanoparticle library approach[34−36] represents a powerful methodology for discovering effective binders[37] and biocompatible nanoparticles[38,39] or for exploring nanostructure−activity relationships (NSAR).[40] In this work, we established a combinatorial nanoparticle library approach to reveal major molecular interaction components for pollutant adsorption using PFOS as an example. We determined that the optimal molecular adsorption of PFOS by functionalized gold nanoparticles (GNPs) requires simultaneous electrostatic and fluorine−fluorine (F−F) interactions. The optimized PFOS-binding GNPs perform well in simulated environmental wastewater.

MATERIALS AND METHODS

Synthesis of Ligands and the GNPs Library. The **SN**, **SH**, and **SF** ligands were synthesized following the routes shown in Schemes S1 and S2. The pK_a values of **SN1−3** were calculated using ACD/I-Lab (https://ilab.acdlabs.com/iLab2/). The dual GNPs library was prepared following the route shown in Scheme S3. The GNPs library was purified by the centrifugation method. Information about the entire dual GNP library is shown in Table 1.

Zeta Potential Measurements. GNPs were suspended in water with sonication. The zeta potentials of the GNPs were measured at 25 °C and at pH 6.0 and pH 11.0 using a Malvern Zetasizer instrument (Malvern Nano ZS90; Malvern Instruments Ltd., Worcestershire, UK). All samples were measured at the same concentration. Each sample was measured in triplicate.

Kinetics Experiments. Adsorption kinetics experiments were performed in 1.5 mL polypropylene centrifuge tubes at pH 6.0 or pH 11.0 at 25 °C on an orbital shaker (240 rpm). In each tube, 0.05 mg of GNPs and 20 μg mL^{-1} PFOS were used. Sampling was performed at 0, 5, 15, 30, 60, 120, and 180 min. After shaking for 120 min, the mixtures were separated by centrifugation.

PFOS Adsorption by GNP Library. PFOS absorption experiments were conducted in 1.5 mL polypropylene centrifuge tubes at pH 6.0 or pH 11.0 at 25 °C on an orbital shaker (240 rpm). All experiments were conducted in triplicate, and the average value was recorded. A PFOS solution without nanoparticles was used as a control.

PFOS Quantification by LC/MS/MS. Following the adsorption experiments, the mixtures were separated by centrifugation. The supernatant was collected and diluted for the determination of the remaining PFOS. The PFOS analysis was conducted on a LC/MS/MS (API 3200; Applied Biosystems/MDS Sciex, Framingham, MA, USA) operated in negative-ion mode. The separation was carried out on a Dionex Acclaim 120 C_{18} column (4.6 mm i.d. × 150 mm length, 5 μm; Dionex China Ltd., Sunnyvale, CA, USA). A 10 min dualistic gradient at a flow rate of 1.0 mL min^{-1} was used. The mobile phases were 50 mM NH_4OAc and water. The elution conditions were as follows: 0 min, 28% NH_4OAc; 3 min, 28% NH_4OAc; 4 min, 5% NH_4OAc; 7 min, 5% NH_4OAc; 8 min, 28% NH_4OAc; 10 min, 28% NH_4OAc. Quantitative analyses were then conducted using ESI/MS/MS (API 3200; Applied Biosystems/MDS Sciex, Framingham, MA, USA). The detection limit was 0.1 ng L^{-1}. The parent/product ions ($PFOS^-/SO_3^-$: 498.8/79.9) were selected as the quantitative ion pair.

RESULTS AND DISCUSSION

Design of a Dual-Ligand PFOS-Targeting Combinatorial GNP Library. We hypothesize that synergistic actions of electrostatic and F−F interactions between PFOS and a solid matrix can maximize molecular interactions for efficient PFOS adsorption (Figure 1). To test this hypothesis, we designed a combinatorial GNP library (Table 1) by varying the length of the poly/perfluoroalkyl chain (containing 4, 7, or 9 carbons, **SH** and **SF**) and amino groups of various pK_a values (pK_a: **SN1**, 9.4 ± 0.4; **SN2**, 9.9 ± 0.4; **SN3**, 10.5 ± 0.4, as calculated by ACD/iLab). With this approach, we can control the protonation of amino groups on GNPs by adjusting the pH values. At pH 11.0, all of the amino groups are not protonated. PFOS molecules likely bind to GNPs through F−F interactions. On the other hand, at pH 6.0, the amino groups on GNPs are all protonated, and PFOS molecules presumably bind to GNPs by both electrostatic and F−F binding interactions. To further compare

DOI: 10.1021/acs.est.7b01635
Environ. Sci. Technol. 2017, 51, 7120−7127

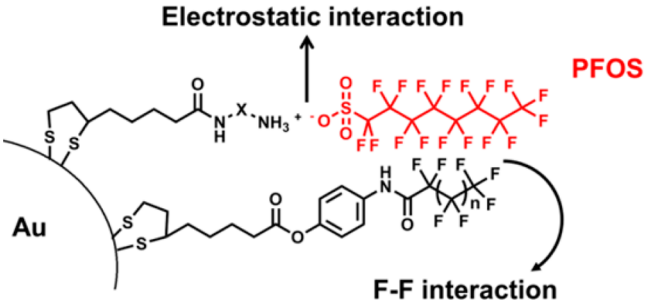

Figure 1. Rationale for the adsorption of PFOS by a dual-ligand GNP.

the PFOS binding strength through F−F interactions with that through hydrophobic interactions, we designed GNPs of similar modifications (the same chain length) with only H atoms replacing the F atoms (Table 1).

Synthesis and Characterization of the PFOS-Targeting GNP Library. Ligands **SN**, **SH**, and **SF** were synthesized following Schemes S1 and S2. The yields of products **SN**, **SH**, and **SF** ranged from 50% to 95%. All products were purified by column chromatography to a purity of ≥95% ($LC/UV_{214\ nm}$) and were characterized by high-resolution mass spectrometry and ^1H NMR (see details in the Supporting Information).

Members of the combinatorial GNP library (**H1**−**H9** and **F1**−**F9**) were synthesized following Scheme S3. The ligands were coupled to GNPs in situ through strong chelation between sulfur and gold atoms. The average number of ligands on each nanoparticle was determined to be 294 ± 25; the **SN**/**SH** and **SN**/**SF** ratios were approximately 1:1 according to LC/MS analysis after ligand cleavage by I_2 (Figure S1, Table S1).[41]

The particle sizes were characterized by TEM (Figure 2a,b). The average diameter of GNPs was 5.0 ± 0.3 nm. The typical size distribution of GNPs is shown in Figure 2c,d. The electrostatic properties of GNPs in aqueous solution strongly affect both their stabilities and their interactions with PFOS. To check the different electrostatic properties of GNPs, the zeta potential of the GNPs in water was determined at both pH 6.0 and pH 11.0. All 18 members exhibited a positive zeta potential at pH 6.0 (15.7 to 31.4 mV) due to the protonation of the amino group (Figure 2e). At pH 11.0, although the surface charge (surface potential) for all GNPs was neutral, they had a negative zeta potential value (−37.2 to −44.1 mV, Figure 2e). Unlike surface potential, which is defined as the potential between the particle surface and the bulk solution, the definition of zeta potential is the potential between the double layer (slipping plane) and the bulk. At the alkaline pH, the surface potential of the amine-functionalized nanoparticles is neutral. However, OH^- ions are accumulated in the first adsorbed layer because of the high pH value. The second layer contains some polarized water molecules. However, these molecules cannot reverse the negative charge from the first layer. Therefore, the zeta potential of our nanoparticles, as well as many other neutral NPs, is negative in agreement with that reported by other researchers.[27,42−46] Because of the different surface potentials at different pH ranges, we might have an opportunity to investigate the adsorption of PFOS only through F−F interactions at pH 11.0 or through the combined F−F and electrostatic interactions at pH 6.0.

Thermodynamic and Kinetics Behavior of PFOS Binding. To understand PFOS adsorption by GNPs, we selected **F6** and **H6** GNPs as models and investigated the isotherm and kinetics of PFOS binding. In order to explore the PFOS binding mechanism, the equilibrium adsorption data were fitted to both Freundilch and Langmuir models. R^2 values of the curve fitting for **F6** were 0.96 vs 0.92 by Freundlich and Langmuir models at pH 6.0. For **H6**, these values were 0.96 vs 0.95. At pH 11.0, such two pairs of values were 0.98 vs 0.97 and 0.99 vs 0.97 (Figure S2). Because of the small differences between these fitting results, we only speculate a possibility that multiple bindings might occur due to the strong F−F interactions; i.e., when a single layer of PFOS molecules bind to the surface of GNPs, extra PFOS molecules could still assume some interactions with the bound PFOS layer.

The time-dependent PFOS adsorption onto **F6** and **H6** GNPs was also determined (Figure S3). In the absence of electrostatic interactions at pH 11.0, rapid adsorption of the

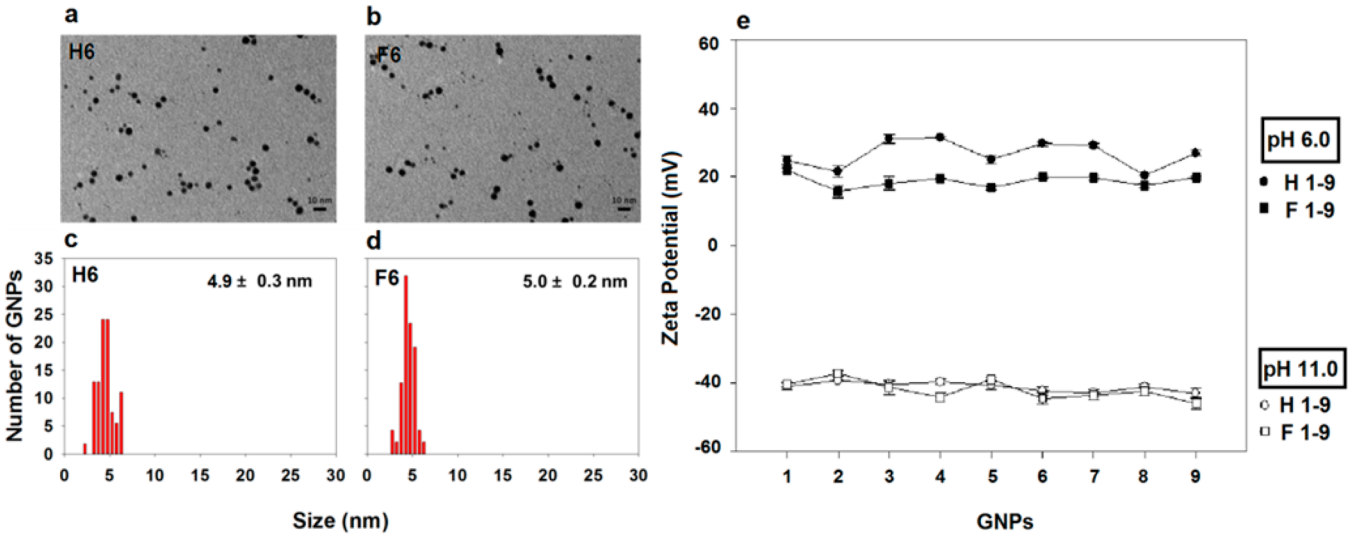

Figure 2. Characterization of selected members (**H6**, **F6**) from the combinatorial GNP library. TEM images of GNP library members **H6** (a) and **F6** (b); the scale bar represents 10 nm. Size distribution of GNPs **H6** (c) and **F6** (d) as measured by TEM; (e) zeta potential of the GNPs in water. The concentration of the liquid was quantified as 50 $\mu g\ mL^{-1}$ and was then measured 3 times independently after balancing for 2 min. Error bars represent ± standard deviation.

DOI: 10.1021/acs.est.7b01635
Environ. Sci. Technol. 2017, 51, 7120−7127

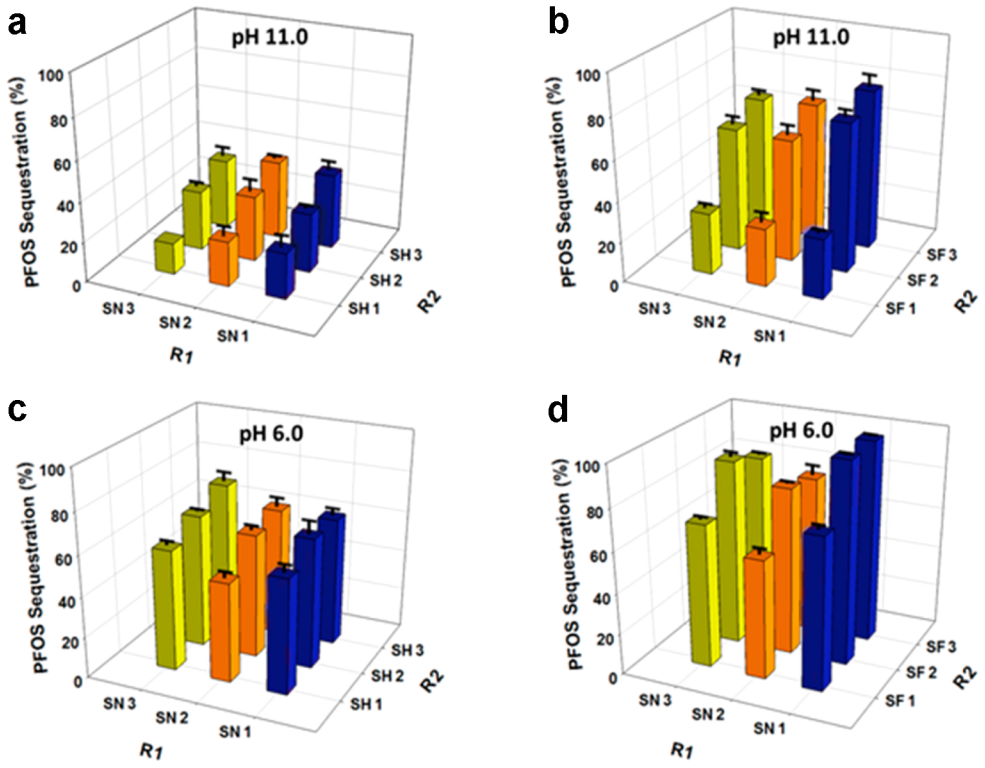

Figure 3. The adsorption of PFOS by the GNP library at pH 11.0 and pH 6.0. (a, b) PFOS adsorption by GNPs was performed at pH 11.0, where **SN** ligands were not protonated (not charged). (c, d) PFOS adsorption by GNPs was performed at pH 6.0, where **SN** ligands were protonated. PFOS (20 μg mL^{-1}) was incubated with GNPs (0.7 mg mL^{-1}) for 120 min before the PFOS concentration in the supernatant was determined. PFOS (20 μg mL^{-1}) in tubes without adding nanoparticles was used as control for correcting PFOS loss due to tube adsorption. The average of three independent measurements is plotted. Error bars represent the standard deviation.

PFOS was observed and equilibrium was reached within 20 min. At pH 6.0, with the additional electrostatic interactions, the binding equilibrium for both kinds of GNPs was reached even faster (Figure S3). At both pH values, faster adsorption was found for **F6** than **H6**. In comparison, the nonspecific adsorption of PFOS onto sediment and soil slowly reaches equilibrium within days,[47,48] and the binding equilibrium of PFOS to MIP adsorbents is reached in 20 h.[25] These results indicate that PFOS adsorption by **F6** was by far the fastest compared to PFOS adsorption by other reported adsorption materials.

Nanostructure-Dependent PFOS Bindings by GNP Library. We further examined the PFOS adsorption efficiency by the GNP library. Although PFOS binding was fast, we still incubated nanoparticles with PFOS for an extended time (120 min) at room temperature before separating them from the supernatant by centrifugation. The concentrations of PFOS in the supernatants were quantified using LC/MS/MS (Figure S4).

To identify the unique GNP−PFOS interactions, we intentionally synthesized GNPs containing surface ligands with a perfluoroalkyl chain (**F1**−**F9**) or a hydrocarbon chain (**H1**−**H9**). In alkaline solution (pH 11.0), the amino groups on both types of GNPs (**H** series and **F** series) are not protonated. PFOS molecules could bind to GNPs only through interactions with the hydrocarbon or perfluoroalkyl chains of the surface ligands. In all experiments, we used only PFOS (20 μg mL^{-1}) without adding nanoparticles as control for correcting the nonspecific PFOS loss due to tube adsorption. GNPs functionalized with hydrocarbon ligands (**H1**−**H9**) exhibited PFOS binding efficiencies ranging from 15% to 39% of the starting PFOS concentration (Figure 3a). Although the PFOS binding efficiency generally increased with increasing chain length of the surface ligands, the PFOS adsorption efficiencies of **F1**−**F9** were nearly doubled (28−79%) compared to those of **H1**−**H9** (15−39%) with hydrocarbon ligands of the same chain lengths (Figure 3b).

The electrostatic interaction between GNPs and PFOS is also an important driving force in addition to the aforementioned F−F or hydrophobic interactions. The **SN** ligands on 18 GNPs were all protonated at pH 6.0. With both electrostatic and F−F (or CF-CH) binding mechanisms, the **H** series exhibited a PFOS binding efficiency of 48% to 71% (Figure 3c), whereas the PFOS binding efficiency of the **F** series ranged from 57% to 98% (Figure 3d). Considering that the PFOS adsorption efficiency at pH 11.0 was primarily due to F−F (for **F**) or hydrophobic (for **H**) interactions, the extra PFOS adsorption might correspond to contributions from the additional electrostatic interactions. On the basis of this simplified dissection, we calculated the percentages of electrostatic vs F−F or hydrophobic interactions (Table 2). The data show that the ratio of electrostatic interactions over F−F/hydrophobic interactions between the GNPs and PFOS was only slightly higher when the latter was relatively weak (such as **F1**−**F3** or **H1**−**H3**). When the hydrocarbon or fluoroalkyl chain became longer (such as in **F7**−**F9** or **H7**−**H9**), the F−F or hydrophobic interactions equalized or overpowered the electrostatic interactions. In the case of **F7**−**F9**, the strength of the F−F interactions was approximately four times stronger than that of the electrostatic interactions. This finding again demonstrated that, although charge interaction was a strong

DOI: 10.1021/acs.est.7b01635
Environ. Sci. Technol. 2017, 51, 7120−7127

Table 2. Key Molecular Determinants for PFOS Binding

	PFOS binding (%)		dissected contributor		
f-GNPs	pH 11.0	pH 6.0	hydrophobic (%)	F−F	electrostatic (%)
H1	22.8 ± 6.6	56.3 ± 5.5	41	—	59
H2	22.5 ± 5.0	48.6 ± 4.5	46	—	54
H3	15.6 ± 0.0	59.1 ± 3.0	26	—	74
H4	29.6 ± 1.5	63.9 ± 7.8	46	—	54
H5	32.7 ± 5.8	60.8 ± 3.0	54	—	46
H6	29.9 ± 1.7	65.4 ± 0.1	46	—	54
H7	37.6 ± 4.2	63.0 ± 4.1	60	—	40
H8	39.2 ± 1.1	63.1 ± 5.1	62	—	38
H9	35.0 ± 4.1	71.4 ± 5.7	49	—	51
Fl	29.7 ± 1.3	74.0 ± 2.9	—	40	60
F2	28.8 ± 4.8	57.9 ± 3.3	—	50	50
F3	30.6 ± 1.8	69.7 ± 2.1	—	44	56
F4	73.8 ± 3.2	98.5 ± 0.2	—	45	55
F5	60.6 ± 4.9	81.4 ± 0.3	—	75	25
F6	61.3 ± 3.7	89.8 ± 3.1	—	68	32
F7	79.4 ± 5.9	98.9 ± 0.3	—	80	20
F8	68.4 ± 4.8	76.9 ± 5.3	—	89	11
F9	66.8 ± 2.5	83.0 ± 0.6	—	80	20

addition for the binding, F−F binding was still a dominant mechanism for PFOS adsorption in an optimal PFOS binder.

Further Analysis of PFOS Binding Components by Computational Chemistry. To explore the molecular mechanisms of the optimal PFOS binding, we used the structural information on the surface ligands to develop a computational model for PFOS binding affinities. Because the GNPs used in this study contain two surface ligands with a 1:1 ratio, we averaged the 11 descriptors related to the surface properties (Figure S5) to obtain values for each pair of ligands for GNPs. Using multilinear regression (MLR) analysis, we developed two MLR models based on the experimental results obtained at two different pH values. The correlation between experimental and calculated PFOS binding values is shown in Figure 4. The results showed that the linearity was good and that the models correctly predicted a higher PFOS adsorption at lower pH (pH 6.0) and higher PFOS binding values by **F1−F9** compared to **H1−H9**.

Because GNP **H1−H9** and GNP **F1−F9** show significant differences in their PFOS bindings, we not only calculated the significance of these 11 descriptors in both models but also calculated different contributions of these descriptors in GNP **H1−H9** and GNP **F1−F9**, respectively. When the pH was changed from 6.0 to 11.0, the orders of significance of these 11 descriptors to both models also changed. At pH 6.0, the most significant descriptor was the maximum single-bond chain length (b_max1len, Figure S5a); thus, the PFOS molecules' binding affinity to GNP **H1−H9** and GNP **F1−F9** mainly depended on the length of the ligand on each GNP, including both F−F and hydrophobic interactions. At pH 11.0, when the amino group was not protonated, the b_max1len descriptor still ranked as the second most important descriptor, indicating the importance of the surface ligand length. However, the most significant descriptor was the total negative van der Waals surface area (PEOE_VSA_NEG, Figure S5b); thus, the PFOS molecule binding affinity was mainly determined by the negative charge of surface ligands, contributed by F atoms, on GNPs. On the basis of this analysis, it is clear that the dominant interactions was F−F interactions at pH 11.0.

Implication for Environmental Applications. The above evidence, both experimental and theoretical, demonstrated that GNPs with both electrostatic and F−F interactions exhibited stronger bindings with PFOS compared to materials with only one of these interaction mechanisms. To examine this, we quantitatively compared PFOS adsorption by **F6** and that by traditional adsorbents, such as granular activated carbon (GAC), powder activated carbon (PAC), and an anion-exchange resin (AI400) with the same surface area or functional group (Table S3). We found that the adsorption rate of **F6** was 48, 46, and 16 times faster than AI400, GAC, and PAC, respectively, and the PFOS adsorption efficiency of **F6** in 24 h was 1.9, 1.5, and 1.2 times higher than AI400, GAC, and PAC under the same experimental conditions (Figure S6). These results demonstrate that functionalized GNP **F6**, with synergistic (electrostatic and F−F) interactions with PFOS, seemed superior to traditional materials GAC, PAC, and AI400 in terms of adsorption rate and binding efficiency.

In wastewater or natural waters, the effect of ionic strength on the adsorption process cannot be ignored. At pH 6.0, GNPs are positively charged. An increase in ionic strength may lead to a reduction of electrostatic attractions between GNPs and PFOS, resulting in a reduced PFOS adsorption. To examine such effects, we determined PFOS adsorption by GNP **F6** under the influence of a thousand-fold of interfering ions. Although more comprehensive tests are still required in future application studies, in this test, our results showed that the PFOS adsorption by **F6** was reduced only by 4% and 5% by Na^+ and K^+ (Figure 6b).

The optimal ligand composition discovered in this work, when transferred to another matrix, such as certain membranes or solid phase, can be used to treat environmental waters. To evaluate the PFOS removal from wastewater by **F6**, we tested PFOS removal in untreated wastewater from an advanced

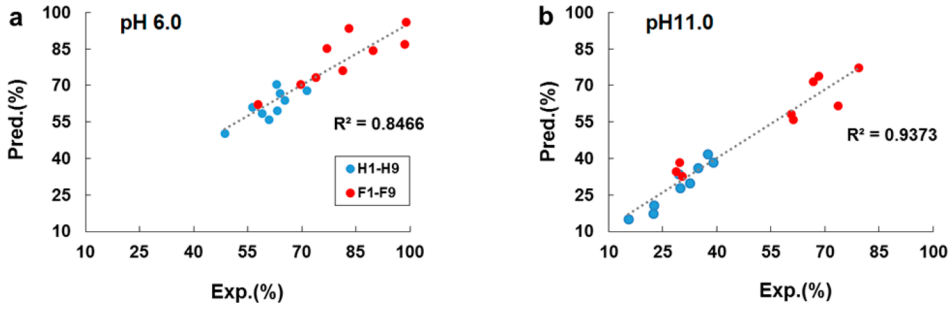

Figure 4. Correlation of experimental and predictive PFOS binding affinity at pH 6.0 (a) and at pH 11.0 (b). GNPs **H1−H9** are indicated in blue and **F1−F9** are shown in red. The R^2 values for the two models are 0.85 and 0.94, respectively.

DOI: 10.1021/acs.est.7b01635
Environ. Sci. Technol. 2017, 51, 7120−7127

wastewater treatment plant near in Beijing (see Supporting Information Materials and Methods). When concentrations of PFOS in wastewater were 2, 5, 50, and 500 $\mu g\ L^{-1}$, **F6** treatment achieved 99.1−87.6% of PFOS removal (Figure 5).

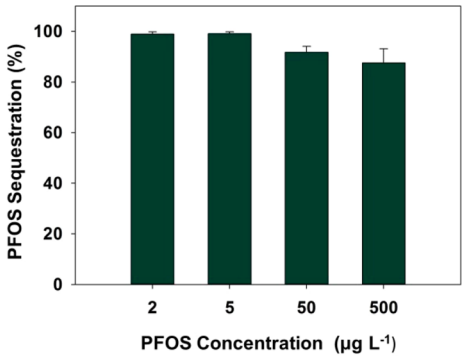

Figure 5. The adsorption of PFOS by the GNP **F6** in wastewater. Standard samples with concentrations of 2, 5, 50, and 500 $\mu g\ L^{-1}$ were incubated with **F6** (0.7 mg mL^{-1}) in wastewater for 120 min at pH 6.0 before the PFOS concentration in the supernatant was determined. The average of three independent measurements is plotted. Error bars represent the standard deviation.

Our results showed that **F6** was quite effective in PFOS adsorption, especially at the lower PFOS concentrations. **F6** treatment of wastewater with starting PFOS concentrations of 2 and 5 $\mu g\ L^{-1}$ resulted in residual PFOS concentrations as low as 22 and 45 ng L^{-1}, well below the U.S. health advisory level for PFOS (70 ng L^{-1}). The PFOS concentration in the environmental water sample treated by **F6** was well below this mark.

In summary, we revealed the major molecular components for optimal PFOS adsorption. The fast binding of PFOS was driven by the interplay of two driving forces between GNPs and PFOS: electrostatic and F−F interactions. The contributions from the former were relatively large when the latter was weak and vice versa. F−F interactions were stronger than regular hydrophobic interactions. These findings may facilitate the future development of PFOS monitoring probes and matrices for removing low concentrations of PFOS. On the basis of these findings, PFOS adsorption can be optimized and applied to environmental treatment, as shown by some feasibility evaluation experiments. The efficient multidimensional testing and elucidation of several key molecular components in PFOS binding using this approach demonstrate the value of the nanoparticle library approach. Although the transformation of the discovered ligands to various matrices for sensor or adsorbent development will be needed, the success of this approach opens an avenue for discovering novel binders of crucial pollutants and for mapping complicated interaction mechanisms between pollutants and binding matrices.

■ ASSOCIATED CONTENT

Supporting Information

The Supporting Information is available free of charge on the ACS Publications website at DOI: 10.1021/acs.est.7b01635.

Materials and methods, schemes of the synthesis of ligands and the GNPs library (Schemes S1−S3), characterization of the ligands on GNPs (Table S1, Figure S1), the isotherm and kinetics of PFOS adsorption by GNPs (Figures S2 and S3), PFOS quantification (Table S2, Figure S4), characteristics of the four absorbents used in this study (Table S3), and implication for environmental applications (Figure S6) (PDF)

■ AUTHOR INFORMATION

Corresponding Authors

*Phone: +86 13969072308; fax: +86 531 88380029; e-mail: drbingyan@yahoo.com.

*E-mail: hyzhou001@gmail.com.

ORCID

Gaoxing Su: 0000-0001-9607-2006

Linlin Zhao: 0000-0002-7283-7681

Bing Yan: 0000-0002-7970-6764

Notes

The authors declare no competing financial interest.

■ ACKNOWLEDGMENTS

We thank Yan Mu for technical assistance. This work was supported by the National Key Research and Development Program of China (2016YFA0203103), the National Natural Science Foundation of China (91543204 and 91643204), and the Strategic Priority Research Program of the Chinese Academy of Sciences (XDB14030401).

■ REFERENCES

(1) Wang, T.; Wang, Y.; Liao, C.; Cai, Y.; Jiang, G. Perspectives on the inclusion of perfluorooctane sulfonate into the Stockholm Convention on Persistent Organic Pollutants. *Environ. Sci. Technol.* **2009**, *43* (14), 5171−5175.

(2) Hansen, K. J.; Johnson, H. O.; Eldridge, J. S.; Butenhoff, J. L.; Dick, L. A. Quantitative characterization of trace levels of PFOS and PFOA in the Tennessee River. *Environ. Sci. Technol.* **2002**, *36* (8), 1681−1685.

(3) Holmström, K. E.; Järnberg, U.; Bignert, A. Temporal trends of PFOS and PFOA in Guillemot eggs from the Baltic Sea, 1968−2003. *Environ. Sci. Technol.* **2005**, *39* (1), 80−84.

(4) Sakurai, T.; Serizawa, S.; Isobe, T.; Kobayashi, J.; Kodama, K.; Kume, G.; Lee, J. H.; Maki, H.; Imaizumi, Y.; Suzuki, N.; et al. Spatial, phase, and temporal distributions of perfluorooctane sulfonate (PFOS) and perfluorooctanoate (PFOA) in Tokyo Bay, Japan. *Environ. Sci. Technol.* **2010**, *44* (11), 4110−4115.

(5) Dorneles, P. R.; Lailsonbrito, J.; Azevedo, A. F.; Meyer, J.; Vidal, L. G.; Fragoso, A. B.; Torres, J. P.; Malm, O.; Blust, R.; Das, K. High accumulation of perfluorooctane sulfonate (PFOS) in marine tucuxi dolphins (Sotalia guianensis) from the Brazilian coast. *Environ. Sci. Technol.* **2008**, *42* (14), 5368−5373.

(6) Inoue, K.; Okada, F.; Ito, R.; Kato, S.; Sasaki, S.; Nakajima, S.; Uno, A.; Saijo, Y.; Sata, F.; Yoshimura, Y.; et al. Perfluorooctane sulfonate (PFOS) and related perfluorinated compounds in human maternal and cord blood samples: Assessment of PFOS exposure in a susceptible population during pregnancy. *Environ. Health Perspect.* **2004**, *112* (11), 1204−1207.

(7) Chen, M. H.; Ha, E. H.; Liao, H. F.; Jeng, S. F.; Su, Y. N.; Wen, T. W.; Lien, G. W.; Chen, C. Y.; Hsieh, W. S.; Chen, P. C. Perfluorinated compound levels in cord blood and neurodevelopment at 2 years of age. *Epidemiology* **2013**, *24* (6), 800−808.

(8) Kowalczyk, J.; Ehlers, S.; Oberhausen, A.; Tischer, M.; Fürst, P.; Schafft, H.; Lahrssenwiederholt, M. Absorption, distribution, and milk secretion of the perfluoroalkyl acids PFBS, PFHxS, PFOS, and PFOA by dairy cows ded naturally contaminated feed. *J. Agric. Food Chem.* **2013**, *61* (12), 2903−2912.

(9) Yeung, W. Y.; Robinson, S.; Koschorreck, J.; Mabury, S. A. Part II. A temporal study of PFOS and its precursors in human plasma from

DOI: 10.1021/acs.est.7b01635
Environ. Sci. Technol. 2017, 51, 7120−7127

two German cities in 1982−2009. *Environ. Sci. Technol.* **2013**, *47* (8), 3875−3882.
(10) Longnecker, M. P.; Smith, C. S.; Kissling, G. E.; Hoppin, J. A.; Butenhoff, J. L.; Decker, E.; Ehresman, D. J.; Ellefson, M. E.; Flaherty, J.; Gardner, M. S.; et al. An interlaboratory study of perfluorinated alkyl compound levels in human plasma. *Environ. Res.* **2008**, *107* (2), 152−159.
(11) Steenland, K.; Tinker, S.; Shankar, A.; Ducatman, A. Association of perfluorooctanoic acid (PFOA) and perfluorooctane sulfonate (PFOS) with uric acid among adults with elevated community exposure to PFOA. *Environ. Health Perspect.* **2010**, *118* (2), 229−233.
(12) Apelberg, B. J.; Witter, F. R.; Herbstman, J. B.; Calafat, A. M.; Halden, R. U.; Needham, L. L.; Goldman, L. R. Cord serum concentrations of perfluorooctane sulfonate (PFOS) and perfluorooctanoate (PFOA) in relation to weight and size at birth. *Environ. Health Perspect.* **2007**, *115* (11), 1670−1676.
(13) Fei, C.; Mclaughlin, J. K.; Lipworth, L.; Olsen, J. Prenatal exposure to perfluorooctanoate (PFOA) and perfluorooctanesulfonate (PFOS) and maternally reported developmental milestones in infancy. *Environ. Health Perspect.* **2008**, *116* (10), 1391−1395.
(14) Cheng, J.; Vecitis, C. D.; Park, H.; Mader, B. T.; Hoffmann, M. R. Sonochemical degradation of peerfluorooctane sulfonate (PFOS) and perfluorooctanoate (PFOA) in landfill groundwater: environmental matrix effects. *Environ. Sci. Technol.* **2008**, *42* (21), 8057−8063.
(15) Rodriguez-Freire, L.; Balachandran, R.; Sierra-Alvarez, R.; Keswani, M. Effect of sound frequency and initial concentration on the sonochemical degradation of perfluorooctane sulfonate (PFOS). *J. Hazard. Mater.* **2015**, *300*, 662−669.
(16) Chularueangaksorn, P.; Tanaka, S.; Fujii, S.; Kunacheva, C. Regeneration and reusability of anion exchange resin used in perfluorooctane sulfonate removal by batch experiments. *J. Appl. Polym. Sci.* **2013**, *130* (2), 884−890.
(17) Xu, C.; Chen, H.; Jiang, F. Adsorption of perflourooctane sulfonate (PFOS) and perfluorooctanoate (PFOA) on polyaniline nanotubes. *Colloids Surf., A* **2015**, *479*, 60−67.
(18) Zhou, Q.; Pan, G.; Zhang, J. Effective sorption of perfluorooctane sulfonate (PFOS) on hexadecyltrimethylammonium bromide immobilized mesoporous SiO 2 hollow sphere. *Chemosphere* **2013**, *90* (9), 2461−2466.
(19) Chen, H.; Zhang, C.; Yu, Y.; Han, J. Sorption of perfluorooctane sulfonate (PFOS) on marine sediments. *Mar. Pollut. Bull.* **2012**, *64* (5), 902−906.
(20) Zhi, Y.; Liu, J. Adsorption of perfluoroalkyl acids by carbonaceous adsorbents: Effect of carbon surface chemistry. *Environ. Pollut.* **2015**, *202*, 168−176.
(21) Chen, X.; Xia, X.; Wang, X.; Qiao, J.; Chen, H. A comparative study on sorption of perfluorooctane sulfonate (PFOS) by chars, ash and carbon nanotubes. *Chemosphere* **2011**, *83* (10), 1313−1319.
(22) Alejandro, S.; Valdés, H.; Manero, M. H.; Zaror, C. A. BTX abatement using Chilean natural zeolite: the role of Brønsted acid sites. *Water Sci. Technol.* **2012**, *66* (8), 1759−1765.
(23) Navarro, I.; Sanz, P.; Martínez, M. Á. Analysis of perfluorinated alkyl substances in Spanish sewage sludge by liquid chromatography-tandem mass spectrometry. *Anal. Bioanal. Chem.* **2011**, *400* (5), 1277−1286.
(24) Perkola, N.; Sainio, P. Survey of perfluorinated alkyl acids in Finnish effluents, storm water, landfill leachate and sludge. *Environ. Sci. Pollut. Res.* **2013**, *20* (11), 7979−7987.
(25) Yu, Q.; Deng, S.; Yu, G. Selective removal of perfluorooctane sulfonate from aqueous solution using chitosan-based molecularly imprinted polymer adsorbents. *Water Res.* **2008**, *42* (12), 3089−3097.
(26) Liu, X.; Yu, Y.; Li, Y.; Zhang, H.; Ling, J.; Sun, X.; Feng, J.; Duan, G. Fluorocarbon-bonded magnetic mesoporous microspheres for the analysis of perfluorinated compounds in human serum by high-performance liquid chromatography coupled to tandem mass spectrometry. *Anal. Chim. Acta* **2014**, *844*, 35−43.
(27) Tenzer, S.; Docter, D.; Kuharev, J.; Musyanovych, A.; Fetz, V.; Hecht, R.; Schlenk, F.; Fischer, D.; Kiouptsi, K.; Reinhardt, C.; et al. Rapid formation of plasma protein corona critically affects nanoparticle pathophysiology. *Nat. Nanotechnol.* **2013**, *8* (10), 772−781.
(28) Yang, L.; Yu, W.; Yan, X.; Deng, C. Decyl-perfluorinated magnetic mesoporous microspheres for extraction and analysis perfluorinated compounds in water using ultrahigh-performance liquid chromatography−mass spectrometry. *J. Sep. Sci.* **2012**, *35* (19), 2629−2636.
(29) Marchetti, N.; Guzzinati, R.; Catani, M.; Massi, A.; Pasti, L.; Cavazzini, A. New insights into perfluorinated adsorbents for analytical and bioanalytical applications. *Anal. Bioanal. Chem.* **2015**, *407* (1), 17−21.
(30) Xu, C.; Zhu, J.; Li, Y.; Yu, Y.; Duan, G. Fluorous solid-phase extraction (F-SPE) as a pilot tool for quantitative determination of perfluorochemicals in water samples coupled with liquid chromatography-tandem mass spectrometry. *RSC Adv.* **2015**, *5* (17), 13192−13199.
(31) Zhang, W. Fluorocarbon stationary phases for liquid chromatography applications. *J. Fluorine Chem.* **2008**, *129* (10), 910−919.
(32) Bacalum, E.; Cheregi, M. Recent analytical applications of fluorinated hydrocarbon-based stationary phases in HPLC. *J. Liq. Chromatogr. Relat. Technol.* **2017**, *40* (2), 59−68.
(33) Du, Z.; Deng, S.; Bei, Y.; Qian, H.; Wang, B.; Huang, J.; Yu, G. Adsorption behavior and mechanism of perfluorinated compounds on various adsorbents—A review. *J. Hazard. Mater.* **2014**, *274* (12), 443−454.
(34) Su, G.; Yan, B. Nano-combinatorial chemistry strategy for nanotechnology research. *J. Comb. Chem.* **2010**, *12* (2), 215−221.
(35) Zhang, B.; Pai, P. A.; Yan, B. A nano-combinatorial approach to developing cancer diagnostics: nano-combinatorial diagnostics discovery. *Nanomedicine* **2012**, *7* (7), 937−940.
(36) Zhou, H.; Mu, Q.; Gao, N.; Liu, A.; Xing, Y.; Gao, S.; Zhang, Q.; Qu, G.; Chen, Y.; Liu, G.; et al. A nano-combinatorial library strategy for the discovery of nanotubes with reduced protein-binding, cytotoxicity, and immune response. *Nano Lett.* **2008**, *8* (3), 859−865.
(37) Zhou, H.; Jiao, P.; Yang, L.; Li, X.; Yan, B. Enhancing cell recognition by scrutinizing cell surfaces with a nanoparticle array. *J. Am. Chem. Soc.* **2011**, *133* (4), 680−682.
(38) Gao, N.; Zhang, Q.; Mu, Q.; Bai, Y.; Li, L.; Zhou, H.; Butch, E. R.; Powell, T. B.; Snyder, S. E.; Jiang, G.; et al. Steering carbon nanotubes to scavenger receptor recognition by nanotube surface chemistry modification partially alleviates NFκB activation and reduces its immunotoxicity. *ACS Nano* **2011**, *5* (6), 4581−4591.
(39) Wu, L.; Zhang, Y.; Zhang, C.; Cui, X.; Zhai, S.; Liu, Y.; Li, C.; Zhu, H.; Qu, G.; Jiang, G.; et al. Tuning cell autophagy by diversifying carbon nanotube surface chemistry. *ACS Nano* **2014**, *8* (3), 2087−2099.
(40) Fourches, D.; Pu, D.; Li, L.; Zhou, H.; Mu, Q.; Su, G.; Yan, B.; Tropsha, A. Computer-aided design of carbon nanotubes with the desired bioactivity and safety profiles. *Nanotoxicology* **2016**, *10* (3), 374−383.
(41) Zhou, H.; Li, X.; Lemoff, A.; Zhang, B.; Yan, B. Structural confirmation and quantification of individual ligands from the surface of multi-functionalized gold nanoparticles. *Analyst* **2010**, *135* (6), 1210−1213.
(42) Alfimov, A. V.; Aryslanova, E. M.; Chivilikhin, S. A. An analytical model of multi-particle electric double-layer interaction between identical spherical colloid nanoparticles. *Proc. SPIE* **2015**, *9519*, 951911.
(43) Lin, Y. C.; Yu, B. Y.; Lin, W. C.; Lee, S. H.; Kuo, C. H.; Shyue, J. J. Tailoring the surface potential of gold nanoparticles with self-assembled monolayers with mixed functional groups. *J. Colloid Interface Sci.* **2009**, *340* (1), 126−130.
(44) Zhang, Y.; Jiang, J.; Li, M.; Gao, P.; Zhou, Y.; Zhang, G.; Shuang, S.; Dong, C. Colorimetric sensor for cysteine in human urine based on novel gold nanoparticles. *Talanta* **2016**, *161*, 520−527.
(45) Liu, X.; Chen, Y.; Li, H.; Huang, N.; Jin, Q.; Ren, K.; Ji, J. Enhanced Retention and Cellular Uptake of Nanoparticles in Tumors

DOI: 10.1021/acs.est.7b01635
Environ. Sci. Technol. 2017, 51, 7120−7127

by Controlling Their Aggregation Behavior. *ACS Nano* **2013**, *7* (7), 6244−6257.
(46) Nallathamby, P. D.; Lee, K. J.; Xu, X. H. N. Design of Stable and Uniform Single Nanoparticle Photonics for In Vivo Dynamics Imaging of Nanoenvironments of Zebrafish Embryonic Fluids. *ACS Nano* **2008**, *2* (7), 1371−1380.
(47) Pan, G.; Jia, C.; Zhao, D.; You, C.; Chen, H.; Jiang, G. Effect of cationic and anionic surfactants on the sorption and desorption of perfluorooctane sulfonate (PFOS) on natural sediments. *Environ. Pollut.* **2009**, *157* (1), 325−330.
(48) Zhang, R.; Yan, W.; Jing, C. Experimental and molecular dynamic simulation study of perfluorooctane sulfonate adsorption on soil and sediment components. *J. Environ. Sci.* **2015**, *29*, 131−138.

DOI: 10.1021/acs.est.7b01635
Environ. Sci. Technol. 2017, 51, 7120−7127